JBC Papers in Press. Published on October 30, 2015 as Manuscript M115.668749
The latest version is at http://www.jbc.org/cgi/doi/10.1074/jbc.M115.668749

Alternative Spliced Isoforms of K_V10.1 Potassium Channels Modulate Channel Properties and can Activate Cyclin-Dependent Kinase in *Xenopus* Oocytes[*]

Fernanda Ramos Gomes[1,3,4], Vincenzo Romaniello[2,3], Araceli Sánchez[2], Claudia Weber[1], Pratibha Narayanan[1], Maryna Psol[1] and Luis A. Pardo[2§].

[1]Department of Molecular Biology of Neuronal Signals and [2]Oncophysiology Group, Max-Planck Institute of Experimental Medicine, Hermann-Rein-Str. 3, 37075 Göttingen, Germany.

[*]Running Title. Alternative splicing of K_V10.1

[3]Equal contributors
[4]Current address: Applied Oncology Group, Max-Planck Institute of Experimental Medicine, Hermann-Rein-Str. 3, 37075 Göttingen, Germany

[§]To whom correspondence should be addressed: Luis A. Pardo, Oncophysiology Group, Max-Planck Institute of Experimental Medicine, Hermann-Rein-Str. 3, 37075 Göttingen, Germany. Tel.: +49 551 3899646; Fax: +49 551 3899644; E-mail: pardo@em.mpg.de

Keywords: potassium channels; RNA splicing; post-transcriptional regulation; glycosylation; cell cycle; K_V10.1; *KCNH1*

ABSTRACT

K_V10.1 is a voltage-gated potassium channel expressed selectively in mammalian brain, but also aberrantly in cancer cells. In this study we identified short splice variants of K_V10.1 resulting from exon skipping events (E65 and E70) in human brain and cancer cell lines. The presence of the variants was confirmed by Northern blot and RNase protection assays. Both variants completely lack the transmembrane domains of the channel, and would produce cytoplasmic proteins without channel function. In a reconstituted system, both variants co-precipitate with the full-length channel and induce a robust down-regulation of K_V10.1 current when co-expressed with the full-length form, but their effect is mechanistically different. E65 requires a tetramerization domain and induces a reduction in the overall expression of full-length K_V10.1, while E70 mainly affects its glycosylation pattern. E65 triggers activation of cyclin-dependent kinases in *Xenopus laevis* oocytes, suggesting a role in cell cycle control. Our observations highlight the relevance of non-canonical functions for the oncogenicity of K_V10.1, which need to be considered when ion channels are targeted for cancer therapy.

The human voltage-gated potassium channel K_V10.1 (*Ether-à-go-go*; *KCNH1*) is physiologically expressed in the brain, where it participates in the control of calcium entry in synapses during repetitive firing (1). It is not detectable in healthy tissues outside of the brain, but its aberrant expression in cancer cells has been repeatedly reported (2,3). This ion channel is involved in cell-cycle progression of tumor cells, whose proliferation can be reduced by inhibition of channel expression (4-6), by treatment with classical channel blockers (7) or also by a functional monoclonal antibody (8). A mutation precluding potassium permeability does not completely abolish xenograft tumor formation by transfected cells (7), indicating that the contribution of K_V10.1 to tumor progression does not fully rely on its primary function as an ion channel. The functional protein is a homo- or heterotetramer, where each monomer is comprised of six transmembrane domains and large cytoplasmic N- and C-termini. Potentially relevant functional domains can be recognized on both

intracellular ends, most prominently calmodulin (CaM) binding domains (9-11), a cyclic nucleotide binding domain (12-15), a Per-Arnt-Sim (PAS) domain in the N-terminus (16,17), a nuclear localization signal (NLS) (18), and a C-terminal tetramerizing coiled-coil (TCC) domain which is relevant for tetrameric assembly (18-21). The function of the channel can be also modified by a number of different interacting proteins, such as (besides CaM) the potassium channel regulator 1 (KCR1), CaM kinase, 14-3-3, epsin, rabaptin 5, cortactin or the PDZ domain protein interacting specifically with TC10 (PIST) (22-28). Mature K_V10.1 channels undergo glycosylation on asparagines 388 (only core glycosylated) and 406 in the extracellular loop between S5 and S6 transmembrane domains (29), shifting the apparent molecular weight from 100kDa to 110kDa and 130kDa, respectively, as assessed by Western blot.
Alternative splicing (AS) is a common post-transcriptional modification leading to expanded proteomic complexity. 95% of multi-exon human genes exhibit AS (30), and so do ion channels. AS resulting in changes in pharmacological profile, electrophysiological properties, surface expression or intracellular localization of ion channels has been described in other channels (31-43). In some cases, the resulting splice variant lacks conductive properties and acts as a dominant-negative (44-46). Two splice variants of the mammalian K_V10.1 have been identified, termed K_V10.1a and K_V10.1b (4,47,48). Both form active ion channels with properties very similar to each other. A third splice variant cloned from *Drosophila* (Eag80) is composed of only the N- and C-termini of the channel. While it does not produce an active ion channel, it activates a signaling cascade leading to altered cell architecture (49). The aim of the present work was to test the occurrence and to study the biological relevance of alternative splicing in human K_V10.1 channels. The knowledge about the contribution of non-canonical ion channel splice variants is crucial to understanding the mechanisms underlying progression and resistance of oncologic diseases.

Experimental procedures

Cells

Cell lines DU145 (ACC 261), HEK 293 (ACC 305), HeLa (ACC 57), IPC 298 (ACC 251), IGR 39 (ACC 239), IMR 32 (ACC 165), and SH-SY5Y (ACC 209) were purchased from DSMZ (Braunschweig, Germany). MDA-MB 435S (HTB 129) cells were from ATCC (Manassas, VA, USA), PNT 2 cells (ECACC95012613) were obtained from ECACC (Salisbury, UK). GL15 cells were kindly provided by Dr. Fioretti (University of Perugia, Italy). Each cell line was cultured in their respective recommended medium supplemented with 10% FCS (PAA Laboratories) at 37 °C in humidified 5% CO_2 atmosphere. For stable transfected cell lines (HEK expressing K_V10.1 in the pTracerCMV vector, a cell line routinely used in our laboratory (4, 6-8), the selection compound Zeocin (Calya) was added to the culture medium at 3µg/mL. Transient transfections were performed using Fugene (Roche Applied Science) or Lipofectamine 2000 (Invitrogen). Proliferation was estimated using Alamar Blue (Biosource) or WST assays (Roche Applied Science) as described (50), or by live cell imaging in an IncuCyte Zoom system (Essen Biosciences) to determine percent confluence as a function of time.

Molecular Biology

The splice variants were cloned in expression vectors by substituting the 1834 bp AarI-BspEI fragment from the relevant plasmids containing K_V10.1 (AarI cuts at exon3, BspEI at exon 11) with the corresponding fragment from the PCR amplicons cloned in pGEM-T (310 bp for E65, 763 bp for E70). The host vectors were pSGEM-K_V10.1 (for efficient expression in the *Xenopus* system) (51), and pcDNA3-K_V10.1 and pcDNA3-K_V10.1-mVenus (18) for expression in mammalian cell lines and generation of the mVenus fusions respectively, where the fluorescent reporter is fused to the C-terminal end of the protein.
Site directed mutagenesis was performed using QuikChange II XL Site-Directed Mutagenesis Kit (Agilent technologies) according to the manufacturer's instruction. Primers for $E65^{L405Y}$ and $E70^{L556Y}$ mutation were:
5'-
AGGAGGACATCAAGGCCTACAACGCCAAA
ATGACCAATA and
5'-
TATTGGTCATTTTGGCGTTGTAGGCCTTGA
TGTCCTCCT

All constructs and amplicons were verified by sequencing.

Total RNA was obtained from cell pellets using RNeasy mini kit (Qiagen), and 2.5 µg of RNA were used for cDNA synthesis using SuperScript First-Strand Synthesis Kit (Invitrogen). RNA and DNA concentration and yield were determined by optical density measurements at 260 and 280 nm using a spectrophotometer (Implen Nanophotometer UV/VIS). Total and Poly A^+ RNA from human brain (hBrain) was purchased from Clontech.

The T7 mMessage mMachine Kit (Ambion) using the T7 promoter from the pSGEM vector was used to prepare cRNA.

K_V10.1 siRNA (Target sequence: 5'-TACAGCCATCTTGGTCCCTTA-3') was designed with the HiPerformance siRNADesign Algorithm (BIOPREDsi). siRNAs (30 nM) were transfected using DreamFect (Oz Biosciences) or nucleofection (Lonza) for electrophysiological experiments (Solution L, programs T020 for IPC 298 and T030 for IGR39). The negative control was the reverse but not complementary ("scrambled") sequence of K_V10.1.

Nested PCR was performed using 1.5 µL first strand cDNA in 25µL reaction volume for 20 cycles (95 °C 30 s, 59 °C 30 s, 72 °C 3 min, with an initial denaturation step of 3 min at 95 °C). 1 µL of the reaction was used as template for the second round (35 cycles). The amplification products were analyzed by electrophoretic separation in agarose gel, followed by cloning in pGEM-T vector and sequencing in all cases.

5' RACE was carried out using the 5'/3' RACE Kit from Roche. 2µg total RNA extracted from melanoma cell lines or commercial human brain RNA (Clontech) were used for cDNA synthesis using external primers 2 and 1, respectively (Table I). The dA-tailed cDNA was amplified at 52 °C using the oligo-dT anchor primer and the specific primer used to synthesize the cDNA. Nested PCR was required to generate a visible product. 1.5 µL of the first round PCR reaction was amplified at 52°C using the anchor oligo-dT and primers internal 1 for the melanoma cell lines, and internal 2 for human brain. The PCR products were gel purified and cloned into pGEM-T Easy vectors (Promega) for sequence analysis. The 3' UTR region was amplified using nested PCR as described above and sequenced. Primers are listed in Table I.

Ribonuclease Protection Assay

Ribonuclease protection assays (RPA) were carried out using the RPA III kit (Ambion) according to the manufacturer's instructions. Briefly, a K_V10.1 cDNA fragment (342 bp for E65 and 197 bp for E70) encompassing the specific exon junctions for each variant was generated by PCR from plasmid DNA, subcloned into pSGEM and the plasmid used as template to synthesize ^{32}P-labeled RNA probe (MAXIscript kit, Ambion). 200,000 cpm purified ^{32}P-labeled RNA was hybridized overnight at 42 °C with 3 µg mRNA isolated from confluent tumor cells (using the Micro-FastTrack 2.0 Kit, Invitrogen). Digestion was then performed for 30 min at 37 °C with RNase A/RNase T1 mix (Ambion). 100 µg of yeast total RNA was used as a negative control to test for the presence of probe self-protection bands. The samples were run on a 5% polyacrylamide gel and exposed for 1–4 days.

Northern-Blot

For separation of mRNA a 2% formaldehyde MOPS-agarose gel was used and left running for 7 hours, the bands were transferred to a Hybond N membrane overnight and cross-linked (UV Stratalinker 1800- Stratagene, 1200 J). The dry membrane was washed with 2x SSC for 10 minutes, pre-hybridized with Rapid-hybr-Buffer (Roche) for 2-3 hours, and incubated overnight at 65 °C with a 700 bp C-terminal [^{32}P]dCTP-labeled K_V10.1 fragment in Rapid-hybr-Buffer plus. The probe was generated using Deca Label DNA Labeling Kit (Fermentas) and purified with IllustraMicroSpin G-50 Columns (GE Healthcare). After overnight hybridization the membrane was collected and washed twice (30 min each) with 2x SSC and again twice with 2x SSC + 0.1% SDS at 65 °C. The membrane was then exposed for 4 hours or overnight.

Immunofluorescence

Rabbit polyclonal anti-K_V10.1 antibodies were generated in our laboratory and have been described elsewhere (2). The polyclonal antibody (#9391) and mAb33 recognize the C-terminus of K_V10.1, while mAb62, binds to the extracellular S5-S6 linker. ToPro3 (Invitrogen) was used to

label nuclei. Briefly, cells were washed thrice with TBS (150 mM NaCl, 20 mM Tris-HCl; pH 7.5), fixed with 4% *p*-formaldehyde (4°C for 4 min), and permeabilized with 1% Triton X-100 in TBS for 10 min. Nonspecific binding was blocked with 10% bovine serum albumin in TBS for 30 min. Primary antibody (1 µg/mL) incubation was done at room temperature for 2 h. AlexaFluor 546–labeled anti-mouse IgG antibody (Molecular Probes) was used as a secondary antibody. The coverslips were mounted using ProLong (Molecular Probes) and observed in a Zeiss LSM 510 Meta laser-scanning confocal microscope.

Protein extraction, separation and western blot

To obtain cell lysates, cultures were washed twice with phosphate-buffered saline and incubated in 3 mL of lysis buffer (mM: 50 Tris-HCl pH 7.4, 300 NaCl, 5 EDTA, 1% Triton X-100 containing protease inhibitor cocktail (Roche)) for 30 min and centrifuged for 15 min at 21,300 x*g*. The supernatant was used as total cell extract. Protein concentration was determined using BCA Protein Assay Reagent (Pierce).
To obtain oocyte lysates, 15 oocytes were incubated in 300 µL oocyte lysis buffer (1% Triton X-100, 150 mM NaCl, 20 mM Tris-HCl, 5 mM MgCl, 5 mM EDTA) for 30 min and centrifuged twice for 2 min at 21,300 x*g*.
Immunoprecipitations were performed using Protein G Magnetic Beads (New England BioLabs). 1 mg protein extract was incubated with the relevant antibody: mAb33 (3 µg, overnight incubation), mAb62 and anti-*Xenopus* Cyclin B2 (Santa Cruz Biotechnology).
Proteins were separated by SDS-PAGE (NuPAGE Novex TRIS Acetate 3-8 % gel; Invitrogen) and transferred to nitrocellulose membranes (GE Healthcare). The membranes were probed with polyclonal 9391 anti-K_V10.1 (dilution 1/1500) or 6551 anti-GFP (dilution 1/1000, Abcam) and developed using Millipore Immobilon system. Signals were detected in a Bio-Rad Chem-Doc luminescence detection system.

Glycosidase digestion

200 µg of protein lysate were immunoprecipitated as described above. The magnetic beads containing the immunoprecipitated proteins were resuspended in 2 µL elution solution (100 mM β-mercaptoethanol in 0.1% SDS). Samples were then heated up to 99 °C for 10 min, briefly centrifuged, and exposed to a magnetic field. At this point, the 21 µL supernatant from each sample were distributed in three microcentrifuge tubes, for treatment with 1µL Endo H (5 U/mL, Sigma), 1µL PNGase F (≥2 U/mL, Sigma), and a control tube (CTL), containing immunoprecipitated samples not treated with enzyme.
The tubes were incubated overnight at 37 °C and then the protein was separated by SDS-PAGE as described above.

Cdc2 Kinase Activity

Oocytes extracts were incubated in a solution containing biotinylated MV peptide for 30 min at 30 °C (Cdc2 substrate; MESACUP Cdc2 Kinase Assay Kit, MBL). The mixture was then transferred to a microwell plate coated with anti-phospho MV peptide monoclonal antibody (4A4). The retained biotinylated phospho MV peptides were subsequently detected with streptavidin-HRP and 3-ethylbenzothiazoline-6-sulphonic acid (ABTS, Invitrogen), measured in a plate reader at 405 nm (reference 490 nm).

Surface labeling

Cells expressing K_V10.1-BBS (52) were incubated for 10 min on ice with 2.5 µg/mL α-Bungarotoxin (BTX)-Biotin (Invitrogen), washed twice with ice-cold PBS, scraped and centrifuged at 800 x *g* for 3 min. Cell pellets were resuspended in 20 mM Tris-HCl, 150 mM NaCl, 5 mM $MgCl_2$, 1% Nonidet-P40, pH 7.4, containing protease inhibitors. The lysates were passed several times through a 25-gauge needle and placed in microcentrifuge tubes, incubated for 20 min on ice and finally centrifuged at 16,100 x *g* for 15 min at 4 °C. Streptavidin-coated plates (Thermo Scientific) were washed twice with PBS containing 0.05% Tween 20, 0.1% BSA and 0.1% Triton X-100. 30 and 150 µg of protein (in triplicates) were then incubated for 30 min on ice. The plates were washed twice and then blocked for 30 min with NPE (150 mM NaCl, 5 mM EDTA, 50 mM Tris, 5mM KCl, 1% Nonidet P-40, pH 7.5) containing 1% casein. Anti-K_V10.1 antibody (mAb62) was diluted in NPE with 0.1% casein and used at 2.5 µg/mL for 90 min. The wells were washed 3 times with NPE with 0.1% casein, and blocked again in NPE with 1% casein

for 30 min. Secondary antibody (1:500 ECL HRP-linked anti-mouse IgG (GE Healthcare)) was then incubated for 90 min. After 7 washes with NPE-0.1% casein, peroxidase activity was determined using ABTS as above.

Patch-Clamp

Recordings were performed in the whole-cell configuration using an EPC9 amplifier and Pulse software (HEKA, Germany). Currents were filtered at 10 kHz and digitized at 50 kHz. Patch pipettes were pulled from Corning #0010 glass (World Precision Instruments) to resistances of 2-3 MΩ. Solutions for HEK293-K_V10.1, IPC298 and IGR39 melanoma cells contained the following compounds (in mM): internal, 100 KCl, 45 NMDG, 5 1,1-bis(O-aminophenoxy)ethane-N,N,N,N-tetracetic acid (BAPTA), 5 EGTA, 1 $MgCl_2$, 10 HEPES pH 7.4; external, 160 NaCl, 2.5 KCl, 2 $CaCl_2$, 1 $MgCl_2$, 8 Glucose, 10 HEPES pH 7.4. Series resistance was compensated to ~85%. To determine K_V10.1 current amplitude, we applied a conditioning pulse to -100 mV for 1500 ms to slow down the activation of hEag1, and the outward currents were then elicited by a square depolarization to +40 mV for 500 ms. I-V protocol consisted of 250 ms (or 500 ms) voltage pulses, ranging from +80 mV to -60mV, with 20 mV decrements. To compare voltage-elicited current response between different groups of cells, the current was first normalized to the cell size (as measured by C_{slow}). The resulting current density was averaged from 80 to 90% time of each pulse and plotted against the voltage.

Non-stationary noise analysis was carried out in the outside-out configuration on macropatches of *Xenopus* oocytes injected with the relevant cRNAs (53). This preparation was necessary in order to have enough amounts of current in a membrane patch. Patches were obtained from the membrane of oocytes devoid of vitelline membrane using 0.9-2 MΩ pipettes filled with 100 mM KCl, 10 mM EGTA, 10 mM HEPES, pH 7.2. Currents were sampled at 20 kHz and filtered at 4 kHz. Variance/current plots were constructed using PulseTools software (HEKA) from several hundred consecutive 50 ms depolarizations to +40 mV from a holding potential of -80 mV. The number of available channels N and the single channel current i were determined from the variance *vs.* average macroscopic current (I) plot using the equation :

$$\sigma^2 = \sigma_0^2 + (I \cdot i - \frac{I^2}{N})$$

Where σ_0^2 represents the baseline variance.

Two-electrode voltage-clamp

Oocytes were injected with 50 nL of a 1 ng/µL cRNA solution and kept at 18 °C in ND96 solution (96 mM NaCl, 2 mM KCl, 0.2 mM $CaCl_2$, 2 mM $MgCl_2$, 0.5 mM theophylline, 0.1 mM Gentamycin, 5 mM HEPES, pH 7.5). Currents were recorded 1-3 days after cRNA injection, using a Turbo TEC-10CD amplifier (NPI electronics) at room temperature. The intracellular electrodes had resistances of 0.3-1.5 MΩ when filled with 2 M KCl. The extracellular measuring solution contained (mM): 115 NaCl, 2.5 KCl, 1.8 $CaCl_2$, 10 HEPES/NaOH, pH 7.2. Data acquisition and analysis were performed with the Pulse-Pulse Fit (HEKA Electronics) and IgorPro (WaveMetrics) software packages. Current records were filtered at 1 kHz. The membrane potential was held at -80 mV. In order to characterize current-voltage relationships, an I-V protocol was used, generally consisting of 250 ms voltage pulses, ranging from +80 mV to -60 mV, in 20 mV decrements. To compare voltage-elicited current responses between different groups of oocytes, the average steady state current from 80 to 95% time of the pulse was plotted against the voltage.

Statistics

Data are presented as mean±SEM for the indicated number of experiments. Methods to determine statistical significance are indicated in the corresponding Figure legend.

RESULTS

K_V10.1 variants in melanoma cell lines

Astemizole reduces the proliferation of many cancer cell lines and its effect can be at least in part attributed to inhibition of the K_V10.1 channel (7,54). We wanted to compare the effects of this drug in two different melanoma cell lines, IPC298 and IGR39. As controls for these experiments we

used DMSO and norastemizole, a metabolite of astemizole that does not block K_V10.1. We observed an intense effect of astemizole on the proliferation of IPC298, but no effect on IGR39 cells (Fig. 1A). This would be in agreement to previous reports that IGR39 show little or no K_V10.1 expression (55); however, in our hands both cell lines are K_V10.1-positive (Table II and (6)). To clarify this discrepancy, we set out to test if the channel protein was present in both cell lines. First, we performed immunoprecipitation with a mixture containing two monoclonal antibodies: mAb33, whose epitope maps to the C-terminal end, and mAb62, directed against the pore region. The presence of K_V10.1 in the immunoprecipitate was subsequently tested by Western blot analysis using a polyclonal, C-terminal-directed antibody. A band of the expected size was detected in both cell lines, indicating that K_V10.1 is expressed in both IPC298 and IGR39 cells (Fig. 1B).

We also stained both cell lines with the two mentioned monoclonal anti-K_V10.1 antibodies (Fig. 1C). Both antibodies labeled IPC298 cells with similar efficiency and gave rise to the same patterns. In IGR39 cells, staining with the pore antibody resulted in a clear peripherally distributed signal (Fig. 1C), but the antibody against the C-terminus of K_V10.1 did not produce any signal. The polyclonal C-terminal antibody used for Western blot experiments was generated against the whole C-terminus of the channel, while the epitope for the monoclonal counterpart corresponds to the TCC domain. Therefore, the lack of signal using the monoclonal antibody would indicate that the epitope is either masked or absent in these cells.

Electrophysiology of IPC298 and IGR39 melanoma cell lines

To test whether the expression of K_V10.1 protein has a functional correlate, we studied the electrophysiological properties of IPC298 and IGR39 cell lines by whole cell patch clamp. Representative current traces from both cell lines are shown in Fig. 1D. In IPC298 cells (*middle traces*), depolarization induced a slowly activating, non-inactivating outward current with kinetics compatible with K_V10.1. For comparison, typical K_V10.1 traces from transfected HEK-K_V10.1 cells are also shown (*left traces*). In contrast, IGR39 cells showed a current with faster activation and partial inactivation (*right traces*). This current, kinetically very different from K_V10.1, was blocked by imipramine (not shown) and astemizole (Fig. 1 E), at concentrations reported to block K_V10.1 (56). Most significantly, the current was abolished by treatment with K_V10.1-specific siRNA (6) (Fig. 1F), strongly suggesting that the current detected requires the presence of K_V10.1 mRNA. The siRNA recognizes nucleotides 690-710 of the open reading frame, corresponding to exon 6, which encodes the transmembrane core of the protein. These results prompted the possibility that the differential electrophysiology is related to the presence of different splice variants in IPC298 and IGR39 cell lines.

K_V10.1 splice variants in cancer cells and brain tissue

To screen for candidate K_V10.1 variants, we performed nested PCR on cDNA synthesized using oligo-dT with primers located on exons 2 and 11 (Table I). The predicted PCR product for the full-length channel (we will refer to it as E100, after the predicted protein size) was approximately 1.9 kbp. Besides this product, a prominent band of approximately 0.9 kbp was detected in IPC298 cells and another with 0.5 kbp in IGR39 cells, although the latter cell line also shows the 0.9 kbp band with lesser abundance (Fig. 2A). Cloning and sequencing of the amplicons showed the expected K_V10.1 sequence for E100; in the case of IGR39 cells, analysis of the 0.5 kbp fragment revealed a sequence that stopped at the end of exon 3, skipped exons 4 to 9 and continued at the beginning of exon 10. This would give rise to a protein of approximately 65kDa that we will hereafter name E65. Sequence analysis of the 0.9 kbp fragments revealed that the end of exon 3 was joined with the beginning of exon 8 from K_V10.1. Following the same logic as for E65, we will term this variant E70 (Fig. 2B). In both E65 and E70 the reading frame was conserved, and no new stop codon was generated. The skipped exons encode for the transmembrane domains of the ion channel: translation of this shorter mRNA is expected to produce non-channel proteins, composed only of the N- and C-termini of K_V10.1. Nested PCR was also performed using additional K_V10.1-expressing cancer cell lines as well as normal human brain. E65 was found in DU145, PNT2 and SH-SY5Y

cells. E70 was amplified in SH-SY5Y, IMR32 cells and human brain. GL15, HeLa, MCF7 and MDA MB 435S cells were negative for both splice forms.

The presence of shorter K_V10.1 splice variants was confirmed by Northern blot. Purified mRNAs from human brain, SH-SY5Y and IGR39 cells (30µg) were hybridized to a labeled probe targeting the K_V10.1 C-terminal region (corresponding to exons 9 to 11), which is expected to be shared by all splice isoforms. This probe hybridized with three RNA bands on brain samples: one migrating at ~9kb and two others having electrophoretic mobility of ~5kb and ~3.5kb. The ~9kb band is compatible with full length K_V10.1 transcript (4,57) and was also detected in SH-SY5Y and IGR39 cells (Fig. 2C). All detected alternative splicing forms are expressed at low levels.

We then sought to confirm the presence of E65 and E70 with ribonuclease protection assay. Purified mRNAs isolated from diverse K_V10.1-expressing cancer cell lines were hybridized with radiolabeled antisense probes specifically targeting E65 and E70 transcripts (human brain RNA was not included in this approach for availability reasons). Single-stranded, unprotected mRNAs were digested and the resulting products were separated on a polyacrylamide gel. A 342 nt band, corresponding to length of the E65 probe was detected in IGR39 cells. E70 was detected in IMR32 and SH-SY5Y cell extracts (Fig. 2D). These experiments demonstrated the expression of E65 and E70 transcripts in native systems.

To exclude the presence of alternatively spliced regions or sequence differences in the 5' and 3' untranslated ends of the mRNA, 5' RACE PCR was carried out. Primers located at regions common to all variants (Table I) were used and a unique band of 350 bp (Fig. 2E, left panel) was amplified, whose sequence was identical to the expected K_V10.1 sequence. 3' RACE using either conventional or thermostable polymerases was systematically unsuccessful, arguably because of the abundance of GC-rich sequences (58) in that region of K_V10.1. Nested PCR using primers placed at exon 11 and at the 3' UTR to amplify the 3'UTR boundaries (Table I) produced a single 900 bp band (Fig. 2E, right panel). Sequencing of the amplicon did not reveal divergences from the expected K_V10.1 sequence. In summary, we found no evidence of the presence of alternatively spliced regions at the 5' and 3' ends of IGR 39 cells (not shown) and human brain (Fig. 2).

Physical interaction of E65 and E70 with K_V10.1

In numerous ion channels, splice variants interact with the correspondent full-length channel, modulating its function (37,39,46,59). To test whether K_V 10.1 interacts with E65 and/or E70, we performed co-immunoprecipitation (co-IP) using extracts from HEK cells stably expressing K_V10.1 (7,56) and co-transfected with E65 or E70 constructs tagged with the fluorescent red-shifted GFP-derivative monomeric Venus (mVenus; expected molecular weights of the fusion proteins: 80 and 95 KDa, respectively). When E65mVenus and E70mVenus were immunoprecipitated using an anti-GFP antibody, Western blotting with an antibody against the C-terminus of K_V10.1 (therefore recognizing all isoforms) revealed the presence of a band compatible with full-length K_V10.1. Co-IP with E65mVenus was more efficient than E70mVenus, but both splice variants were able to pull down the full-length protein.

The bands detected were qualitatively different. While E65mVenus pulled a diffuse band similar to the majoritarian form present in the inputs, E70mVenus immunoprecipitates showed two sharper bands of smaller size (Fig. 3A, right panel), compatible with the partially (110 kDa) and fully (100 kDa) deglycosylated forms of the channel, respectively.

The reverse co-IP using a monoclonal anti-K_V10.1 antibody directed against the pore region (which therefore does not bind to any of the shorter variants) developed with anti-GFP antibody revealed the presence of E65mVenus or E70mVenus in the corresponding extract, thus confirming the interaction (Fig. 3B).

We conclude that both E65 and E70 interact with the full-length channel in living cells.

E65 and E70 interaction with K_V10.1 alters the abundance and glycosylation pattern of the full-length channel

The typical K_V10.1 glycosylation pattern (after immunobloting using a specific antibody) consists of two distinct bands, with electrophoretic mobility corresponding to ~110 and ~130 kDa (E110 and E130). E110 corresponds to core glycosylated K_V10.1 located in the ER and Golgi, while E130 is

a post-ER, complex glycosylated species (29). If K_V10.1 is completely deglycosylated by PNGaseF, the apparent size in the gel is ~100 kDa. Co-IP showed different band patterns of full length K_V10.1 depending on which of the isoforms was co-expressed, suggestive of differences in glycosylation (Fig. 4A). To characterize the glycosylation status of the immunoprecipitated bands we used Endo H (that removes only core oligosaccharides) or PNGase F (which fully deglycosylates proteins). The protein pulled down by E65 showed a pattern similar to the full-length form after both treatments. On the other hand, the co-IP with E70 was enriched in the unglycosylated forms, indicated by the limited extent of changes induced by enzymatic treatment (Fig. 4A) suggesting that E70 interacts preferentially with the non-glycosylated full-length channel. When different ratios of full-length K_V10.1 and E70 were injected into *Xenopus* oocytes, the fraction of complex glycosylated full-length version decreased with increasing amount of E70, while the abundance of E110 concomitantly increased (Fig. 4B, C), portending that E70 reduces complete maturation of the full-length protein.

In contrast, E65 did not alter the glycosylation of full-length K_V10.1, but rather affected the total amount of full-length expressed in *Xenopus* oocytes co-injected with both K_V10.1 and E65. The full-length K_V10.1 band was virtually abolished when co-expressed with E65 in 1:10 ratio (Fig. 4D).

The surface expression of K_V10.1 was not diminished by coexpression of E65 or E70. Cells expressing a K_V10.1 containing an extracellular bungarotoxin binding site (K_V10.1BBS) were transfected with E65 or E70 (in pcDNA3) in HEK cells. The cells were treated with BTX on ice to avoid internalization, and bound to BTX was determined by ELISA (Fig. 4E); none of the splice variants induced a reduction of surface labeling as compared to the control cells (non-transfected or transfected with empty vector).

E65 and E70 down-regulate K_V10.1 currents in Xenopus laevis *oocytes and HEK293 cells.*

The interaction of K_V10.1 with short isoforms had also functional impact. When cRNAs encoding for E65 or E70 were injected into *Xenopus* oocytes, the current measured in these oocytes with two-electrode voltage clamp was undistinguishable from the one measured in uninjected oocytes (Fig. 5A). This was expected because both short forms lack the transmembrane segments and should therefore not form functional channels. Co-injection of either E65 or E70 with K_V10.1 cRNA at 1:10 ratio resulted in a strong reduction (85% and 60%, respectively) of the current (Fig. 5B, C). Furthermore, the presence of E65 induced an intense inward rectification: depolarizations to very positive potential induced current amplitudes that were smaller than those induced by less intense stimuli (Fig. 5B, *middle trace*). Neither E65 nor E70 expression influenced massively the appearance or amplitude of current elicited by another voltage-gated potassium channel (K_V1.4; Fig. 5D, E), indicating that the interaction with E65 or E70 is specific for K_V10.1. Although E65 induced a modest reduction (37±16%; p=0.02 at +80 mV; n=18) of the current of K_V1.4, this effect could arguably be explained by the modification that E65 alone induces on the oocyte itself (see below).

The reduction in current amplitude observed in oocytes is unlikely to be due to the specific expression system, because comparable results were obtained from HEK293 cells stably expressing K_V10.1 and transiently co-transfected with E65mVenus or E70mVenus (using mVenus alone as a control) and measured 24-72 hours after transfection in whole cell patch clamp experiments (Fig. 5F, G). mVenus fluorescence was used to select transfected cells for recording. E65 and E70 expression resulted in a marked K_V10.1 current reduction of 41.7 ±20.5% for E65 and 53.8 ±21.1% for E70 ($p<0.0001$, two-way ANOVA, Fig. 5G).

A reduction in the total current measured can be a result of a smaller current through each open channel, a reduced open probability, or a smaller number of available channels, which are not necessarily all that are present on the membrane (which are not or only little changed Fig. 4E). To distinguish between these possibilities, we performed non-stationary noise analysis in membrane patches from oocytes expressing E100 either alone or in combination (at 1:10 ratio) with E65 or E70. As summarized in Figure 5H, neither of the isoforms reduced the open probability at +40 mV (0.48±0.17, 0.46±0.13 and 0.42±0.15 for E100, E100+E65 and E100+E70 respectively). E70 did not either change the single channel current (886±85 fA for E100 *vs.* 829±37 fA for

E100+E70), indicating that the number of available channels is the factor that is reduced in this combination, despite the fact that the total channels on the membrane do not seem to change.
In contrast, E65 did induce a reduction (to 593±42 fA), again pointing to a mechanistically different action of the two variants.

Role of the tetramerization domain in the physical and functional interaction between E65 and E70 and the full-length K_V10.1

The tetramerizing coiled-coil (TCC) domain is a 41 amino acid sequence in the C-terminus of K_V10.1 important for specific and stable tetrameric assembly. A point mutation at position 20 within this sequence (L913Y) disrupts the coiled-coil domain and tetramerization (19). Here, this mutation was used to test the requirement of the TCC motif for the interaction between short isoforms and full-length K_V10.1. E65 and E70 mutated at the corresponding position co-precipitated with K_V10.1, although in $E65^{L405Y}$ co-IP was less efficient than in $E70^{L556Y}$ (Fig. 6A). Therefore, an intact TCC is not required for the physical interaction between isoforms.
K_V10.1 functional properties were also determined when co-expressed with the mutant short variants in whole cell patch clamp experiments (Fig. 6B and C). $E70^{L556Y}$ induced a reduction in K_V10.1 current density by 45.3±20.3% ($p<0.001$, two-way ANOVA) at +80 mV (Fig. 6C), an effect similar to wild type E70. In contrast, $E65^{L405Y}$ reduced current amplitude only slightly, and the difference did not reach statistical significance (20.8 ±21.9%, Fig. 6C). These results strongly suggest that, although TCC is not required for the interaction, it plays a critical role in the E65-induced K_V10.1 current decrease.

E65 expression triggers cell cycle progression in Xenopus *oocytes.*

X. laevis oocytes are physiologically arrested in the late G2 phase of the first meiotic division. Application of progesterone triggers activation of mitosis promoting factor (CyclinB/$p34^{Cdc2}$) and progression to meiosis II in a process called maturation. When K_V10.1 channels are expressed in *Xenopus* oocytes, maturation of the oocyte induces a reduction in current amplitude and a strong inward rectification, due to block by intracellular sodium (60,61). Here we found that the current phenotype resulting from recordings of oocytes co-injected with full-length K_V10.1 and E65 is very similar to the one observed in mature oocytes (Fig. 7A). Such phenotype was detected despite the fact that physiological maturation of the oocytes was inhibited by using theophylline in oocytes medium. We therefore hypothesized that E65 itself could induce maturation of the oocyte. Active Cdc2 present in mature oocytes can trigger the cascade when a cytoplasmic extract of mature oocytes is injected in immature oocytes. When an extract from E65-expressing oocytes was injected into naïve oocytes, (followed by RNase treatment to eliminate the pre-injected cRNA), germinal vesicle breakdown (GVBD), the hallmark of maturation, was detected 2 h post-injection (Fig.7B, Table III). Injection of RNase-treated extracts of control oocytes or of extracts from oocytes injected with E70 did not induce GVBD.
An early and decisive event in the process of physiological maturation of the oocyte is an increase in the abundance of cyclin B2. The action of E65 appears to happen downstream of this step, because induction of maturation by E65 did not require an increase in the levels of Cyclin B2 (Fig. 7C). Indeed, Cyclin B2 levels were unaffected in E65-expressing and naïve oocytes compared to uninjected and E100-injected samples, both before and after the physiological induction of maturation with progesterone (5 µg/mL) (Fig. 7C). Nevertheless, we could detect high Cdc2 kinase activity in E65-expressing oocytes, comparable to the activity observed in progesterone-treated samples (Fig. 7D). This could explain the induction of GVBD. Oocytes injected with E100 showed a lesser Cdc2 kinase activity, and in uninjected oocytes, we did not observe Cdc2 activity (not showed). We conclude that E65 induces maturation of the oocyte by direct activation of Cdc2 without increase in Cyclin B levels. However, we did not observe a consistent and reproducible change in cell cycle distribution in mammalian cells expressing K_V10.1 upon overexpression of E65 or E70 (Data not shown).

Discussion

We have isolated two novel splice variants of K_V10.1. Alternative splicing can induce profound modifications in the properties of proteins, including ion channels. We hypothesized that the

differences between properties of the human melanoma cell lines IGR39 and IPC298 could be due to alternative splicing. IGR39 melanoma cells express K_V10.1 at the transcript and protein level. However, no current with kinetics suggestive of this channel was detected, although the pharmacology of the current in IGR39 cells was similar to that of K_V10.1. Most importantly, the current was abolished by K_V10.1-specific siRNA (Fig. 1F). Based on the immunocytochemistry shown in Fig. 1, our initial hypothesis was the presence of an alternative isoform containing the K_V10.1 pore but not the C-terminal region (Fig. 1C). However, we have not been able to isolate such a variant, but rather a novel short variant (E65) that does contain a canonical C-terminus. It still needs to be unequivocally clarified why the C-terminal region in IGR39 cells is detected in immunoprecipitation but not in immunocytochemistry experiments, but a possible explanation is that the epitope for mAb33 is three-dimensional (our unpublished observations). Human brain expresses a different short isoform (E70), which is also detected in neuroblastoma cell lines and IPC298 melanoma cells.

None of the splice variants could be detected as protein in native systems, and therefore we assume scarce expression, either because their expression is actually low, or because they are only present in a subset of cells. The short variants could represent orthologs of the known Eag80 splice variants described in *Drosophila* (49).

The predicted products of E65 and E70 would bear all functional domains described for the C-terminus, but lack all transmembrane segments and part of the PAS domain. The cyclic nucleotide binding domain and the PAS domain have been described to interact and modulate channel gating (62); the interacting residues are still present in the splice variants, and it is therefore conceivable that the interactions still exist.

Several non-channel proteins resulting from AS events have been described to modulate the biophysical properties of the corresponding full-length channel (37,41,44-46). Both E65 and E70 interact with the full-length K_V10.1, leading to variant-specific biological consequences. E65 causes an overall reduction of K_V10.1 protein level (Fig. 4D) and reduces single channel current, while E70 diminishes the ratio of complex-to-core glycosylated K_V10.1 in a dose-dependent manner (Fig. 4B and 4C) without detectably affecting electrophysiological parameters.

The molecular interaction between the short isoforms and the full-length K_V10.1 could involve heterotetramerization between the isoforms that would render the channel inactive (63) since all four pore loops are required to generate an active channel. Both E65 and E70 retain the TCC domain. However, we found that TCC-defective E65 and E70 short isoforms conserve the interaction with K_V10.1 (Fig. 6A). Consequently, the interaction between short isoforms and full-length channel would occur through other interaction site(s).

Disruption of the coiled structure of the TCC abolished the reduction in current induced by E65, but E70 retained the ability to diminish the current. This would be consistent with and action of E65 involving interference with K^+ permeation (thereby reducing conductance) while E70 rather reduces the amount of channels that that can be activated, although the overall abundance of membrane channels is not affected by either isoform. Lack of proper glycosylation is known to render inactive channels, even if this happens after the channels have been inserted in the plasma membrane (29). Therefore, an impairment of Kv101 glycosylation would be enough to explain the observations with E70.

The effect of E65 requires a more complex interpretation. Beside a strongly reduced amount of K_V10.1 current, *Xenopus laevis* oocytes co-expressing K_V10.1 and E65 show a dramatic voltage-dependent inward rectification that can be explained because E65 induces the activation of Cdc2 independently of Cyclin B (Fig. 7C and 7D). Injection of full-length channel alone also induces a significant increase in Cdc2 activity, which could be due to processing of the E100 RNA to produce E65 (49), although we have not further tested this hypothesis. Such an effect would potentially affect the measurements depicted in Fig. 5H. Although rectification in mature oocytes is a phenomenon attributable in this case to block by intracellular sodium (61) and this cation was not present in the internal solution, the reduction in single channel current could be due to the maturation of the oocyte, rather than a direct action of E65 on the channel. The effects on cdc2 activity, although a potentially interesting observation with pathophysiological consequences, fall outside of

the focus of the present study and were not further explored.

Taken together, our results highlight the K_V10.1 complexity of action in the context of tumorigenesis, which can be cell-type (and therefore tumor-) specific, and also underline the relevance of non-canonical effects of ion channels both in physiological (like it is the case of E70 in the brain) and pathological (take for example E65) conditions.

Acknowledgements. We thank W. Stühmer for continued advice and support, K. Decker for help in some experiments, and V. Díaz, K. Dümke and U. Kutzke for technical assistance. VR was supported by a GGNB scholarship.

GenBank accession numbers: KT895501 (E70) and KT895502 (E65).

Conflict of Interest. The authors declare that they have no conflicts of interest with the contents of this article.

Author Contributions. LAP designed research; CW initiated the project; all authors designed, performed and analyzed experiments, FRG, VR, AS, CW and LAP participated in writing the manuscript.

References

1. Mortensen, L. S., Schmidt, H., Farsi, Z., Barrantes-Freer, A., Rubio, M. E., Ufartes, R., Eilers, J., Sakaba, T., Stuehmer, W., and Pardo, L. A. (2015) Kv10.1 opposes activity-dependent increase in Ca^{2+} influx into the presynaptic terminal of the parallel fibre-Purkinje cell synapse. *J Physiol* **593**, 181-196
2. Hemmerlein, B., Weseloh, R. M., de Queiroz, F. M., Knötgen, H., Sánchez, A., Rubio, M. E., Martin, S., Schliephacke, T., Jenke, M., Radzun, H.-J., Stühmer, W., and Pardo, L. A. (2006) Overexpression of Eag1 potassium channels in clinical tumours. *Mol Cancer* **5**, 41 10.1186/1476-4598-5-41
3. Martin, S., De Oliveira, C. L., De Queiroz, F. M., Pardo, L. A., Stuhmer, W., and Del Bel, E. (2008) Eag1 potassium channel immunohistochemistry in the CNS of adult rat and selected regions of human brain. *Neuroscience* **155**, 833-844
4. Pardo, L. A., del Camino, D., Sanchez, A., Alves, F., Brüggemann, A., Beckh, S., and Stühmer, W. (1999) Oncogenic potential of EAG K^+ channels. *EMBO J.* **18**, 5540-5547
5. Gavrilova-Ruch, O., Schönherr, K., Gessner, G., Schönherr, R., Klapperstuck, T., Wohlrab, W., and Heinemann, S. H. (2002) Effects of imipramine on ion channels and proliferation of IGR1 melanoma cells. *J. Membr. Biol.* **188**, 137-149
6. Weber, C., Mello de Queiroz, F., Downie, B. R., Suckow, A., Stuhmer, W., and Pardo, L. A. (2006) Silencing the activity and proliferative properties of the human EagI potassium channel by RNA Interference. *J. Biol. Chem.* **281**, 13030-13037
7. Downie, B. R., Sánchez, A., Knötgen, H., Contreras-Jurado, C., Gymnopoulos, M., Weber, C., Stühmer, W., and Pardo, L. A. (2008) Eag1 expression interferes with hypoxia homeostasis and induces angiogenesis in tumors. *J. Biol. Chem.* **283**, 36234-36240
8. Gómez-Varela, D., Zwick-Wallasch, E., Knötgen, H., Sánchez, A., Hettmann, T., Ossipov, D., Weseloh, R., Contreras-Jurado, C., Rothe, M., Stühmer, W., and Pardo, L. A. (2007) Monoclonal antibody blockade of the human Eag1 potassium channel function exerts antitumor activity. *Cancer Res.* **67**, 7343-7349
9. Schonherr, R., Lober, K., and Heinemann, S. H. (2000) Inhibition of human ether a go-go potassium channels by Ca(2+)/calmodulin. *EMBO J.* **19**, 3263-3271
10. Ziechner, U., Schönherr, R., Born, A.-K., Gavrilova-Ruch, O., Glaser, R. W., Malesevic, M., Küllertz, G., and Heinemann, S. H. (2006) Inhibition of human ether à go-go potassium channels by Ca2+/calmodulin binding to the cytosolic N- and C-termini. *FEBS J.* **273**, 1074-1086
11. Gonçalves, J. T., and Stühmer, W. (2010) Calmodulin Interaction with hEAG1 Visualized by FRET Microscopy. *PloS one* **5**, e10873 10.1371/journal.pone.0010873

12. Brelidze, T. I., Carlson, A. E., and Zagotta, W. N. (2009) Absence of direct cyclic nucleotide modulation of mEAG1 and hERG1 channels revealed with fluorescence and electrophysiological methods. *J. Biol. Chem.* **284**, 27989-27997
13. Brelidze, T. I., Carlson, A. E., Sankaran, B., and Zagotta, W. N. (2012) Structure of the carboxy-terminal region of a KCNH channel. *Nature* **481**, 530-533
14. Muskett, F. W., Thouta, S., Thomson, S. J., Bowen, A., Stansfeld, P. J., and Mitcheson, J. S. (2011) Mechanistic insight into human ether-a-go-go-related gene (hERG) K+ channel deactivation gating from the solution structure of the EAG domain. *J Biol Chem* **286**, 6184-6191
15. Stevens, L., Ju, M., and Wray, D. (2009) Roles of surface residues of intracellular domains of heag potassium channels. *Eur. Biophys. J.* **38**, 523-532
16. Adaixo, R., Harley, C. A., Castro-Rodrigues, A. F., and Morais-Cabral, J. H. (2013) Structural Properties of PAS Domains from the *KCNH* Potassium Channels. *PloS one* **8**, e59265 10.1371/journal.pone.0059265
17. Adaixo, R., and Morais-Cabral, J. H. (2010) Crystallization and preliminary crystallographic characterization of the PAS domains of *EAG* and *ELK* potassium channels. *Acta crystallogr Sect F Struct Biol Cryst Commun* **66**, 1056-1059
18. Chen, Y., Sánchez, A., Rubio, M. E., Kohl, T., Pardo, L. A., and Stühmer, W. (2011) Functional Kv10.1 Channels Localize to the Inner Nuclear Membrane. *PloS one* **6**, e19257 10.1371/journal.pone.0019257
19. Jenke, M., Sanchez, A., Monje, F., Stuhmer, W., Weseloh, R. M., and Pardo, L. A. (2003) C-terminal domains implicated in the functional surface expression of potassium channels. *EMBO J.* **22**, 395-403
20. Lin, T. F., Lin, I. W., Chen, S. C., Wu, H. H., Yang, C. S., Fang, H. Y., Chiu, M. M., and Jeng, C. J. (2014) The Subfamily-specific Assembly of Eag and Erg K+ channels is determined by both the amino and the carboxyl recognition domains. *J. Biol. Chem.* **289**, 22815-22834
21. Ludwig, J., Owen, D., and Pongs, O. (1997) Carboxy-terminal domain mediates assembly of the voltage-gated rat ether-a-go-go potassium channel. *EMBO J.* **16**, 6337-6345
22. Herrmann, S., Ninkovic, M., Kohl, T., Lörinczi, E., and Pardo, L. A. (2012) Cortactin controls surface expression of the voltage-gated potassium channel K_V10.1. *J. Biol. Chem.* **287**, 44151-44163
23. Herrmann, S., Ninkovic, M., Kohl, T., and Pardo, L. A. (2013) PIST (GOPC) modulates the oncogenic voltage-gated potassium channel Kv10.1. *Front Physiol* **4**, 201 10.3389/fphys.2013.00201
24. Hoshi, N., Takahashi, H., Shahidullah, M., Yokoyama, S., and Higashida, H. (1998) KCR1, a membrane protein that facilitates functional expression of non-inactivating K^+ currents associates with rat EAG voltage-dependent K^+ channels. *J. Biol. Chem.* **273**, 23080-23085
25. Hsu, P.-H., Miaw, S.-C., Chuang, C.-C., Chang, P.-Y., Fu, S.-J., Jow, G.-M., Chiu, M.-M., and Jeng, C.-J. (2012) 14-3-3 is a binding partner of rat eag1 potassium channels. *PloS one* **7**, e41203 10.1371/journal.pone.0041203
26. Ninkovic, M., Mitkovski, M., Kohl, T., Stühmer, W., and Pardo, L. A. (2012) Physical and functional interaction of K_V10.1 with Rabaptin-5 impacts ion channel trafficking. *FEBS Lett.* **586**, 3077-3084
27. Piros, E. T., Shen, L., and Huang, X. Y. (1999) Purification of an EH domain-binding protein from rat brain that modulates the gating of the rat ether-a-go-go channel. *J. Biol. Chem.* **274**, 33677-33683
28. Sun, X. X., Hodge, J. J. L., Zhou, Y., Nguyen, M., and Griffith, L. C. (2004) The eag potassium channel binds and locally activates calcium/calmodulin-dependent protein kinase II. *J. Biol. Chem.* **279**, 10206-10214
29. Napp, J., Monje, F., Stuhmer, W., and Pardo, L. A. (2005) Glycosylation of Eag1 (Kv10.1) potassium channels: intracellular trafficking and functional consequences. *J. Biol. Chem.* **280**, 29506-29512

30. Barash, Y., Calarco, J. A., Gao, W., Pan, Q., Wan, X., Shai, O., Blencowe, B. J., and Frey, B. J. (2010) Deciphering the splicing code. *Nature* **465**, 53-59
31. Chen, L., Tian, L., MacDonald, S. H. F., McClafferty, H., Hammond, M. S. L., Huibant, J. M., Ruth, P., Knaus, H. G., and Shipston, M. J. (2005) Functionally diverse complement of large conductance calcium- and voltage-activated potassium channel (BK) alpha-subunits generated from a single site of splicing. *J. Biol. Chem.* **280**, 33599-33609
32. Erxleben, C., Everhart, A. L., Romeo, C., Florance, H., Bauer, M. B., Alcorta, D. A., Rossie, S., Shipston, M. J., and Armstrong, D. L. (2002) Interacting effects of N-terminal variation and strex exon splicing on slo potassium channel regulation by calcium, phosphorylation, and oxidation. *J. Biol. Chem.* **277**, 27045-27052
33. Fletcher, E. V., Kullmann, D. M., and Schorge, S. (2011) Alternative splicing modulates inactivation of type 1 voltage-gated sodium channels by toggling an amino acid in the first S3-S4 linker. *J. Biol. Chem.* **286**, 36700-36708
34. Guasti, L., Crociani, O., Redaelli, E., Pillozzi, S., Polvani, S., Masselli, M., Mello, T., Galli, A., Amedei, A., Wymore, R. S., Wanke, E., and Arcangeli, A. (2008) Identification of a posttranslational mechanism for the regulation of hERG1 K^+ channel expression and hERG1 current density in tumor cells. *Mol. Cell. Biol.* **28**, 5043-5060
35. Kupershmidt, S., Snyders, D. J., Raes, A., and Roden, D. M. (1998) A k+ channel splice variant common in human heart lacks a c-terminal domain required for expression of rapidly activating delayed rectifier current. *J. Biol. Chem.* **273**, 27231-27235
36. McCartney, C., McClafferty, H., Huibant, J., Rowan, E., Shipston, M., and Rowe, I. (2005) A cysteine-rich motif confers hypoxia sensitivity to mammalian large conductance voltage- and Ca-activated K (BK) channel alpha-subunits. *Proc Natl Acad Sci U S A.* **102**, 17870-17876
37. Ohya, S., Niwa, S., Yanagi, A., Fukuyo, Y., Yamamura, H., and Imaizumi, Y. (2011) Involvement of dominant-negative spliced variants of the intermediate conductance Ca2+-activated K+ channel, K(Ca)3.1, in immune function of lymphoid cells. *J. Biol. Chem.* **286**, 16940-16952
38. Schroeter, A., Walzik, S., Blechschmidt, S., Haufe, V., Benndorf, K., and Zimmer, T. (2010) Structure and function of splice variants of the cardiac voltage-gated sodium channel Nav1.5. *J Mol Cell Cardiol* **49**, 16-24
39. Tan, B. Z., Jiang, F., Tan, M. Y., Yu, D., Huang, H., Shen, Y., and Soong, T. W. (2011) Functional characterization of alternative splicing in the C terminus of L-type Cav1.3 channels. *J. Biol. Chem.* **286**, 42725-42735
40. Tian, L., Duncan, R. R., Hammond, M. S., Coghill, L. S., Wen, H., Rusinova, R., Clark, A. G., Levitan, I. B., and Shipston, M. J. (2001) Alternative splicing switches potassium channel sensitivity to protein phosphorylation. *J. Biol. Chem.* **276**, 7717-7720
41. Wagner, V., Stadelmeyer, E., Riederer, M., Regitnig, P., Gorischek, A., Devaney, T., Schmidt, K., Tritthart, H. A., Hirschberg, K., Bauernhofer, T., and Schreibmayer, W. (2010) Cloning and characterisation of GIRK1 variants resulting from alternative RNA editing of the KCNJ3 gene transcript in a human breast cancer cell line. *J. Cell. Biochem.* **110**, 598-608
42. Zarei, M. M., Eghbali, M., Alioua, A., Song, M., Knaus, H. G., Stefani, E., and Toro, L. (2004) An endoplasmic reticulum trafficking signal prevents surface expression of a voltage- and Ca^{2+}-activated K^+ channel splice variant. *Proc Natl Acad Sci U S A.* **101**, 10072-10077
43. Zhang, H. Y., Liao, P., Wang, J. J., Yu, D. J., and Soong, T. W. (2010) Alternative splicing modulates diltiazem sensitivity of cardiac and vascular smooth muscle Cav1.2 calcium channels. *Br. J. Pharmacol.* **160**, 1631-1640
44. Bidaux, G., Beck, B., Zholos, A., Gordienko, D., Lemonnier, L., Flourakis, M., Roudbaraki, M., Borowiec, A. S., Fernandez, J., Delcourt, P., Lepage, G., Shuba, Y., Skryma, R., and Prevarskaya, N. (2012) Regulation of activity of transient receptor potential melastatin 8 (TRPM8) channel by its short isoforms. *J. Biol. Chem.* **287**, 2948-2962
45. Chu, X., Tong, Q., Wozney, J., Zhang, W., Cheung, J. Y., Conrad, K., Mazack, V., Stahl, R., Barber, D. L., and Miller, B. A. (2005) Identification of an N-terminal TRPC2 splice variant which inhibits calcium influx. *Cell Calcium* **37**, 173-182

46. Veale, E. L., Rees, K. A., Mathie, A., and Trapp, S. (2010) Dominant negative effects of a non-conducting TREK1 splice variant expressed in brain. *J. Biol. Chem.* **285**, 29295-29304
47. Frings, S., Brull, N., Dzeja, C., Angele, A., Hagen, V., Kaupp, U. B., and Baumann, A. (1998) Characterization of ether-a-go-go channels present in photoreceptors reveals similarity to IKx, a K+ current in rod inner segments. *J. Gen. Physiol.* **111**, 583-599
48. Warmke, J. W., and Ganetzki, B. (1994) A family of potassium channel genes related to eag in *Drosophila* and mammals. *Proc. Natl. Acad. Sci. U.S.A.* **91**, 3438-3442
49. Sun, X. X., Bostrom, S. L., and Griffith, L. C. (2009) Alternative splicing of the eag potassium channel gene in Drosophila generates a novel signal transduction scaffolding protein. *Mol. Cell. Neurosci.* **40**, 338-343
50. Hartung, F., Stühmer, W., and Pardo , L. A. (2011) Tumor cell-selective apoptosis induction through targeting of KV10.1 via bifunctional TRAIL antibody. *Mol Cancer* **10**, 109 10.1186/1476-4598-10-109
51. Camacho, J., Sánchez, A., Stühmer, W., and Pardo, L. A. (2000) Cytoskeletal interactions determine the electrophysiological properties of human EAG potassium channels. *Pflugers Arch* **441**, 167-174
52. Kohl, T., Lörinczi, E., Pardo, L. A., and Stühmer, W. (2011) Rapid Internalization of the Oncogenic K+Channel Kv10.1. *PloS one* **6**, e26329 10.1371/journal.pone.0026329
53. Heinemann, S. H., and Conti, F. (1992) Nonstationary noise analysis and application to patch clamp recordings. *Methods Enzymol.* **207**, 131-148
54. de Guadalupe Chávez-López, M., Hernández-Gallegos, E., Vázquez-Sánchez, A. Y., Gariglio, P., and Camacho, J. (2014) Antiproliferative and proapoptotic effects of astemizole on cervical cancer cells. *Int J Gynecol Cancer* **24**, 824-828
55. Meyer, R., Schonherr, R., Gavrilova-Ruch, O., Wohlrab, W., and Heinemann, S. H. (1999) Identification of ether a go-go and calcium-activated potassium channels in human melanoma cells. *J. Membr. Biol.* **171**, 107-115
56. García-Ferreiro, R. E., Kerschensteiner, D., Major, F., Monje, F., Stühmer, W., and Pardo, L. A. (2004) Mechanism of block of hEag1 K^+ channels by imipramine and astemizole. *J. Gen. Physiol.* **124**, 301-317
57. Occhiodoro, T., Bernheim, L., Liu, J.-H., Bijlenga, P., Sinnreich, M., Bader, C. R., and Fischer-Lougheed, J. (1998) Cloning of a human ether-a-go-go potassium channel expressed in myoblasts at the onset of fusion. *FEBS Lett.* **434**, 177-182
58. Shi, X., and Jarvis, D. L. (2006) A new rapid amplification of cDNA ends method for extremely guanine plus cytosine-rich genes. *Anal. Biochem.* **356**, 222-228
59. Chiu, Y. H., Alvarez-Baron, C., Kim, E. Y., and Dryer, S. E. (2010) Dominant-negative regulation of cell surface expression by a pentapeptide motif at the extreme COOH terminus of a Slo1 calcium-activated potassium channel splice variant. *Mol. Pharmacol.* **77**, 497-507
60. Brüggemann, A., Stühmer, W., and Pardo, L. A. (1997) Mitosis-promoting factor-mediated suppression of a cloned delayed rectifier potassium channel expressed in Xenopus oocytes. *Proc Natl Acad Sci USA* **94**, 537-542
61. Pardo, L. A., Bruggemann, A., Camacho, J., and Stuhmer, W. (1998) Cell cycle-related changes in the conducting properties of r-eag K+ channels. *J. Cell Biol.* **143**, 767-775
62. Haitin, Y., Carlson, A. E., and Zagotta, W. N. (2013) The structural mechanism of KCNH-channel regulation by the eag domain. *Nature* **501**, 444-448
63. Kuzhikandathil, E. V., and Oxford, G. S. (2000) Dominant-negative mutants identify a role for GIRK channels in D3 dopamine receptor-mediated regulation of spontaneous secretory activity. *J. Gen. Physiol.* **115**, 697-706

Figure Legends

Figure 1. K_V10.1 protein detection in melanoma cell lines. (A) Astemizole (red symbols) reduces proliferation (measured as percent confluence) in melanoma cell lines as compared to norastemizole (blue symbols) and vehicle control (black symbols). Both drugs were used at 500 nM. In IPC298 cells the proliferation was strongly reduced by astemizole treatment, while in IGR39 cells there was no effect. (B) The cell extracts were precipitated using a mixture of two anti-K_V10.1 monoclonal antibodies (mAb33 against the C-terminus and mAb62 against the pore region of the channel) and detected with an anti-K_V10.1 polyclonal antibody. (C) K_V10.1 immunostaining using mAb33 (*upper panel*) and mAb62 (*lower panel*) for IGR39 (*left*) and IPC298 (*right*) melanoma cell lines. (D) K_V10.1 currents elicited in HEK293-K_V10.1 (*left traces*), IPC298 (*middle traces*) and IGR39 (*right traces*) cell lines. HEK293-K_V10.1 (n=21), IPC298 (n=82) and IGR39 (n=121). (E) Reduction on K_V10.1 currents by 5µM Astemizole. Current amplitides were determined as mean current in the last 100 ms of a 1.3 s depolarization to +60 mV for 9 (IPC298, *left*) and 10 cells (IGR39, *right*) (F) Reduction on K_V10.1 currents by a K_V10.1 siRNA. Cells were transfected with siRNA for K_V10.1 and currents measured after 30 hours as described for (E). The graphs (*left panel*) IPC298 (scrambled n=8, siRNA n=11) and (*right panel*) IGR39 (scrambled n=9, siRNA n=10) show that more than 80% of the current was blocked by the siRNA against K_V10.1. ****; $p<0.0001$.

Figure 2. Detection of K_V10.1 splice variants in human cell lines and brain tissue. (A) 1.5% agarose gel with nested PCR products obtained with the specific primers for K_V10.1 listed in Table I. Lane 1 and 2: cDNAs for IPC298 and IGR39 cells, respectively. Lane 3: blank. (B) Scheme of the exon structure of K_V10.1 - E100 and the splice variants E65 and E70. (C) Northern blot analysis of variant mRNA expression in human tissues and human cells**.** 30 µg of mRNA from the cell lines and tissues indicated were separated in a 2% formaldehyde agarose gel, transferred to Hybond-N membranes and hybridized overnight to a 700 bp DNA probe for the C-terminus of K_V10.1 channel (^{32}P-C-terminus). (D) Detection of E65 and E70 splice variant by ribonuclease protection assay. Two antisense ^{32}P-labeled RNA probes (342bp for E65and 197bp for E70) were hybridized with mRNA isolated from tumor cells. The probes protected from RNases digestion were analyzed by polyacrylamide gel electrophoresis and autoradiography. The 342bp (*left panel*) and the 197bp (*right panel*) protected fragment represent the 3-10 and the 3-8 exon junctions, respectively. (E) 5'RACE (*left panel*) and 3'UTR amplification (*right panel*) in human brain tissue. The amplified products from RACE amplifications and 3'UTR nested PCR were separated in 1,5% agarose gel.

Figure 3. E65 and E70 co-precipitate with E100. (A) Right panel: immunoprecipitation of mVenus isoforms with anti-GFP antibody co-precipitated E100 protein of ~130 kDa and ~110 kDa in E100 + E65 samples and E100 protein of ~110 kDa and ~100 kDa in E100 + E70 samples. Left panel: input samples consisting of 10% (20 µg) not immunoprecipitated cell extracts. (B) Right panel: immunoprecipitation of E100 with a K_V10.1 transmembrane domain-targeting antibody co-precipitated E65 and E70 proteins of ~65 kDa and ~70 kDa in E100+E65 and E100+E70 samples, respectively. Left panel: input samples consisting of 10% (20 µg) not immunoprecipitated cell extracts. As detection antibody anti-GFP was used in both left and right panel.

Figure 4. Analysis of E100 glycosylation upon co-expression with E65 and E70. (A) Co-immunoprecipitation with an anti-K_V10.1 monoclonal antibody (mAb33) of E100 with the short isoforms E65 and E70 was performed and precipitates were digested using Endo H and PNGase F to highlight the E100 glycosylation pattern. Notice that E130 is virtually absent when E100 is coexpressed with E70. (B) Immunoprecipitation of E100 and E70 proteins in oocytes injected with increasing ratios E70-E100. E110/E130 ratio increases together with increasing ratios of E70/ full length channel cRNA injected. (C) Densitometry analysis of data in Fig. 4B. (D) Immunoprecipitation of E100 with the short isoform E65

performed in oocyte lysates (15) using an anti-K_V10.1 monoclonal antibody (mAb33) and detected with an anti- K_V10.1 polyclonal antibody. Notice that E100 is strongly reduced when coexpressed with E65 at a 1:10 ratio. (E). Surface expression of the full-length form is not reduced by the spliced variants. Cells expressing a K_V10.1 carrying an extracellular BTX binding site were labeled with biotinylated BTX, and the amount of label incorporated was quantified by sandwich ELISA (n=9).

Figure 5. K_V10.1 current is down-regulated on co-expression with E65 and E70 in two different heterologous expression systems. (A) E65 or E70 alone fail to generate potassium currents in oocytes. Traces were obtained from oocytes injected with E70, E65 or uninjected. None of the conditions gave rise to significant potassium currents. (B) Representative current traces for full length K_V10.1 (E100; *left panel*), E100+E65 (*middle panel*) and E100+E70 (*right panel*) from voltage clamp experiments in *Xenopus* oocytes. (C) Current-voltage relationship for E100 (black circles, n=20), E100+E65 (red squares, n=16) and E100+E70 (blue triangles, n=20). (D) Current traces obtained from oocytes expressing K_V1.4 either alone or together with E65 or E70. Current kinetics was not altered by coexpression. (E) Current-voltage relationship in oocytes expressing K_V1.4 together with E65 or E70 1:10. E70 had no detectable effects on the current (n=24), while E65 induced a modest reduction (37 ±16%; p=0.02 at +80 mV; n=18). The effects of E65 alone on the properties of the oocytes could be responsible in part of this phenomenon. (F) Representative traces from patch clamp experiments**:** HEK cells stably expressing E100 and transfected with either mVenus (*left panel*), E65mVenus (*middle panel*) or E70mVenus (*right panel*). Only green fluorescent cells visualized under epifluorescence microscopy were used for recordings. (G) Current-voltage relationship for HEK-K_V10.1 (E100, black circles, n=12), E100+E70 (blue triangles, n=11) and E100+E65 (red squares n=13). *: p<0.05; **: p<0.01; ***: p<0.001. H. Representative plots of variance *vs.* mean current for K_V10.1 (black), K_V10.1+ E65 (red) and K_V10.1+E70 (blue), both injected at 1:10 ratio. The parameters resulting in the fit shown are detailed in the text.

Figure 6. TCC is not necessary for interaction between K_V10.1 and the splice variant E70 but impairs the current reduction induced by E65. (A) Immunoprecipitation of mVenus-fused splice variants $E65^{L405Y}$ and $E70^{L556Y}$ transiently expressed in HEK cells with anti-GFP antibody co-precipitated K_V10.1 protein (~130 kDa). *Input*: 10% (20 µg) cell extracts. (B) Patch clamp recordings of HEK cells: typical current traces from transfected cells co-expressing either mVenus (*left panel*), E100+$E65^{L405Y}$mVenus (*middle panel*) or E100+$E70^{L556Y}$mVenus (*right panel*). Only green fluorescent cells visualized under epifluorescence microscope were used for recordings. (C) I-V graph representing the mean current density at each voltage step for HEK- K_V10.1 transfected with mVenus (black circles), $E65^{L405Y}$mVenus (red squares) and $E70^{L556Y}$mVenus (blue triangles). *: p<0.05; ***: p<0.001)

Figure 7. Expression of E65 in *Xenopus* oocytes induces oocyte maturation independently of Cyclin B and increases Cdc2 kinase activity. (A) I-V relationship corresponding to the current for E100 (black), E100+E65 in 1:10 ratio (red) and E100 + progesterone pulse (open circles). ***: p<0.001; asterisks apply for both full length K_V10.1+E65 and progesterone pulse. (B) GVBD was visible in oocytes injected with RNase-treated extract from E65-expressing oocytes (*right panel*), but not with RNase-treated extract from uninjected oocytes (*left panel*) or injected with extract from E70-injected oocytes (*middle panel*). (C) Extracts from näive (*upper panel*) or mature (progesterone-treated, *lower panel*) oocytes (n=15) injected with the indicated cRNA combinations were immunoprecipitated and immunoblotted using an anti-Cyclin B2 monoclonal antibody. (D) Cdc2/Cdk1 activity was determined by ELISA under the described conditions. ****:p<0.0001.

Table I: Sequences of primers used

	Primers	Sequence
Nested PCR		
	External Forward	5'-TGT TCG GCG GTC CAA TGA TAC TAA-3'
	External Reverse	5'-TCC CGG CCC CCT CTC TCA-3'
3’ UTR		
	External Forward	5’-ACC GTG CGT GAG AGT CCT-3’
	External Reverse	5’-TTC TCG GCA CTT TCC CAC C-3’
	Internal Forward	5’-GGC AGC CTC CAC CTC CG-3’
	Internal Reverse	5’-ATG GCT GCT GCT CTG TTC TG-3’
5’ RACE		
	External 1	5’-TGC AGATCA CAG TAG GTC AAG GC-3’
	External 2	5’-AAT CCA TTA CTC GCT CAC TCA-3’
	Internal 1	5’-TTC AAT CGT GTC TTT ATC AG-3’

Table II: K_V10.1 expression in human brain and melanoma cell lines (assessed by real-time PCR).

Cell Line	K_V10.1 expression normalized to hTfR	Standard Deviation
Human brain	1.195	0.097
Melanoma IGR39	0.058	0.007
Melanoma IPC298	0.031	0.002

Table III: Germinal Vesicle Break Down (GVBD).

Treatment	Injected oocytes	Visible GVBD	Not evaluable
E65 extract	109	64	13
E70 extract	20	--	--
Uninjected extract	80	--	10
K_V10.1 cRNA	30	--	--

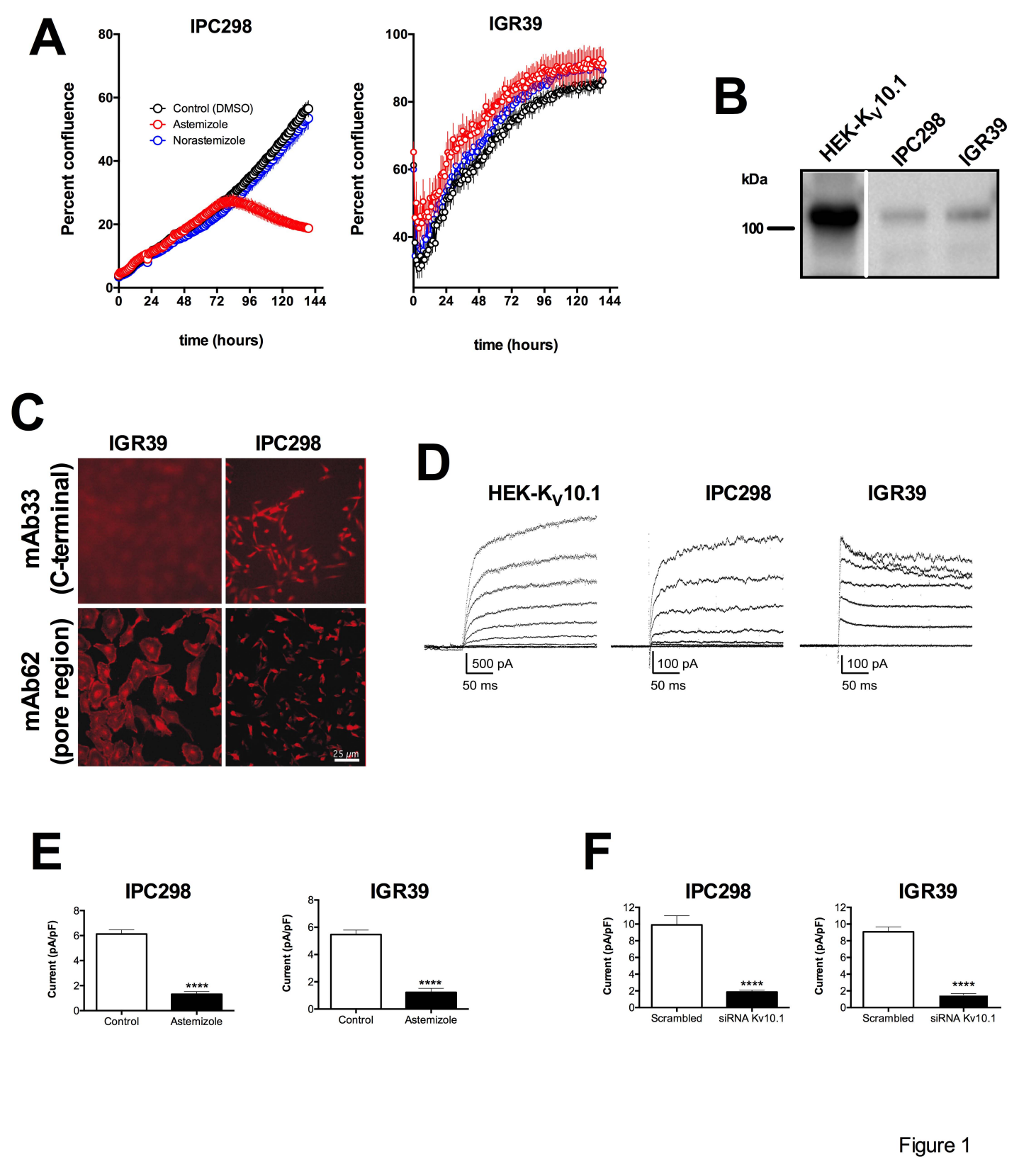
A
IPC298
IGR39
Percent confluence
time (hours)
Control (DMSO)
Astemizole
Norastemizole
B
HEK-Kv10.1
IPC298
IGR39
kDa
100
C
IGR39
IPC298
mAb33 (C-terminal)
mAb62 (pore region)
25 µm
D
HEK-Kv10.1
IPC298
IGR39
500 pA
100 pA
50 ms
E
IPC298
IGR39
Current (pA/pF)
****
Control
Astemizole
F
IPC298
IGR39
Scrambled
siRNA Kv10.1

Figure 1

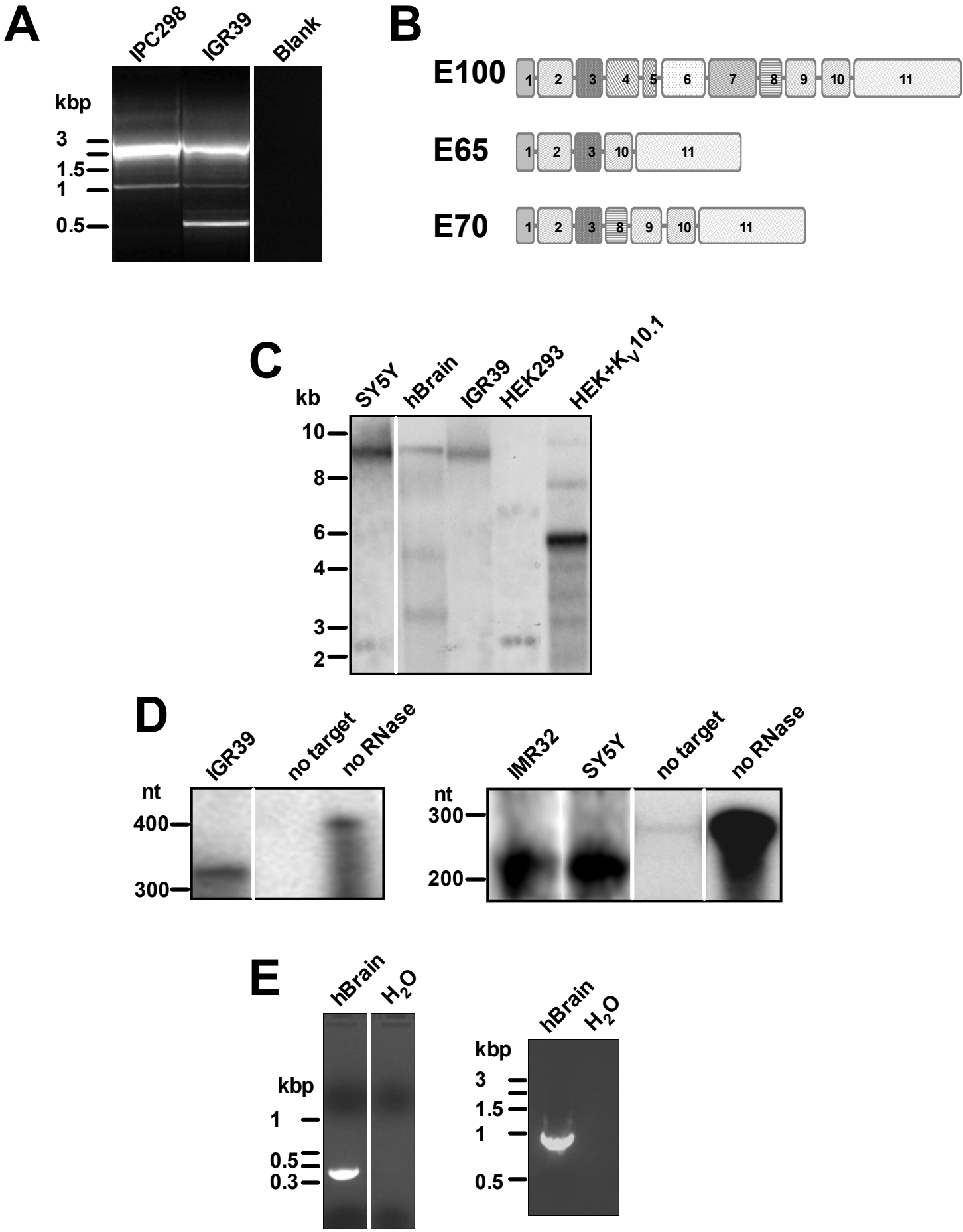
A
IPC298
IGR39
Blank
kbp
3
1.5
1
0.5
B
E100
1
2
3
4
5
6
7
8
9
10
11
E65
1
2
3
10
11
E70
1
2
3
8
9
10
11
C
kb
SY5Y
hBrain
IGR39
HEK293
HEK+K$_V$10.1
10
8
6
4
3
2
D
IGR39
no target
no RNase
nt
400
300
IMR32
SY5Y
no target
no RNase
nt
300
200
E
hBrain
H$_2$O
kbp
1
0.5
0.3
hBrain
H$_2$O
kbp
3
1.5
1
0.5

Figure 2

A

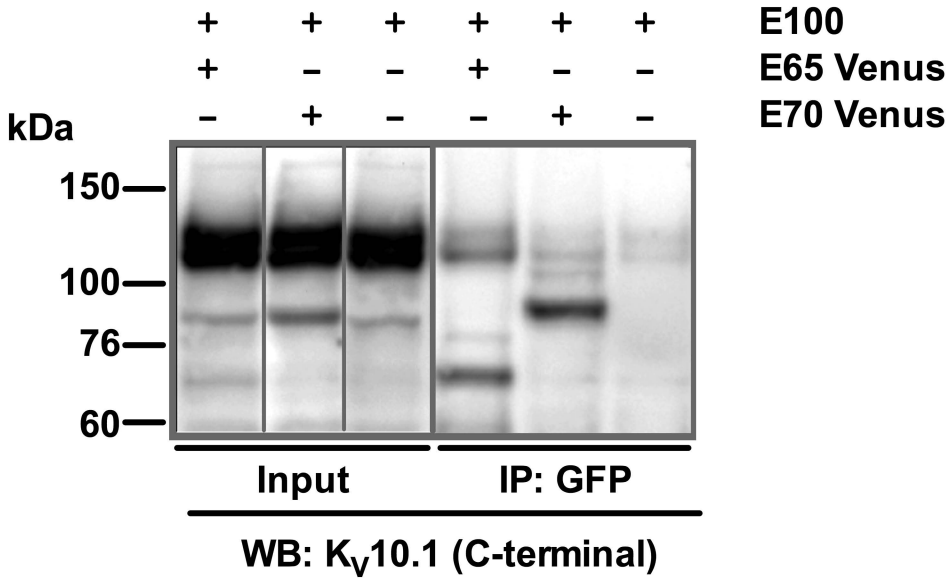
+ + + + + + E100
+ – – + – – E65 Venus
– + – – + – E70 Venus
kDa
150
100
76
60
Input
IP: GFP
WB: K_V10.1 (C-terminal)

B

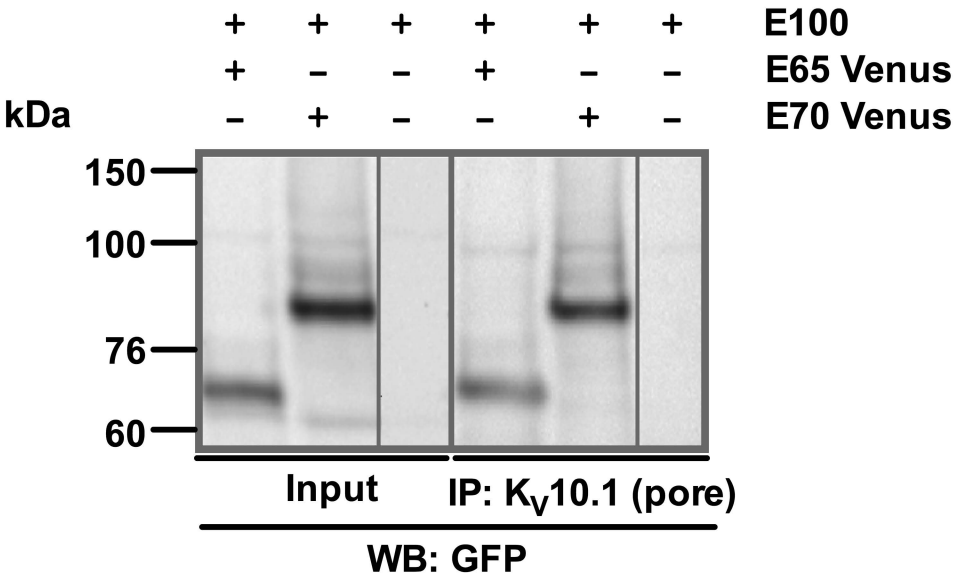
+ + + + + + E100
+ – – + – – E65 Venus
– + – – + – E70 Venus
kDa
150
100
76
60
Input
IP: K_V10.1 (pore)
WB: GFP

Figure 3

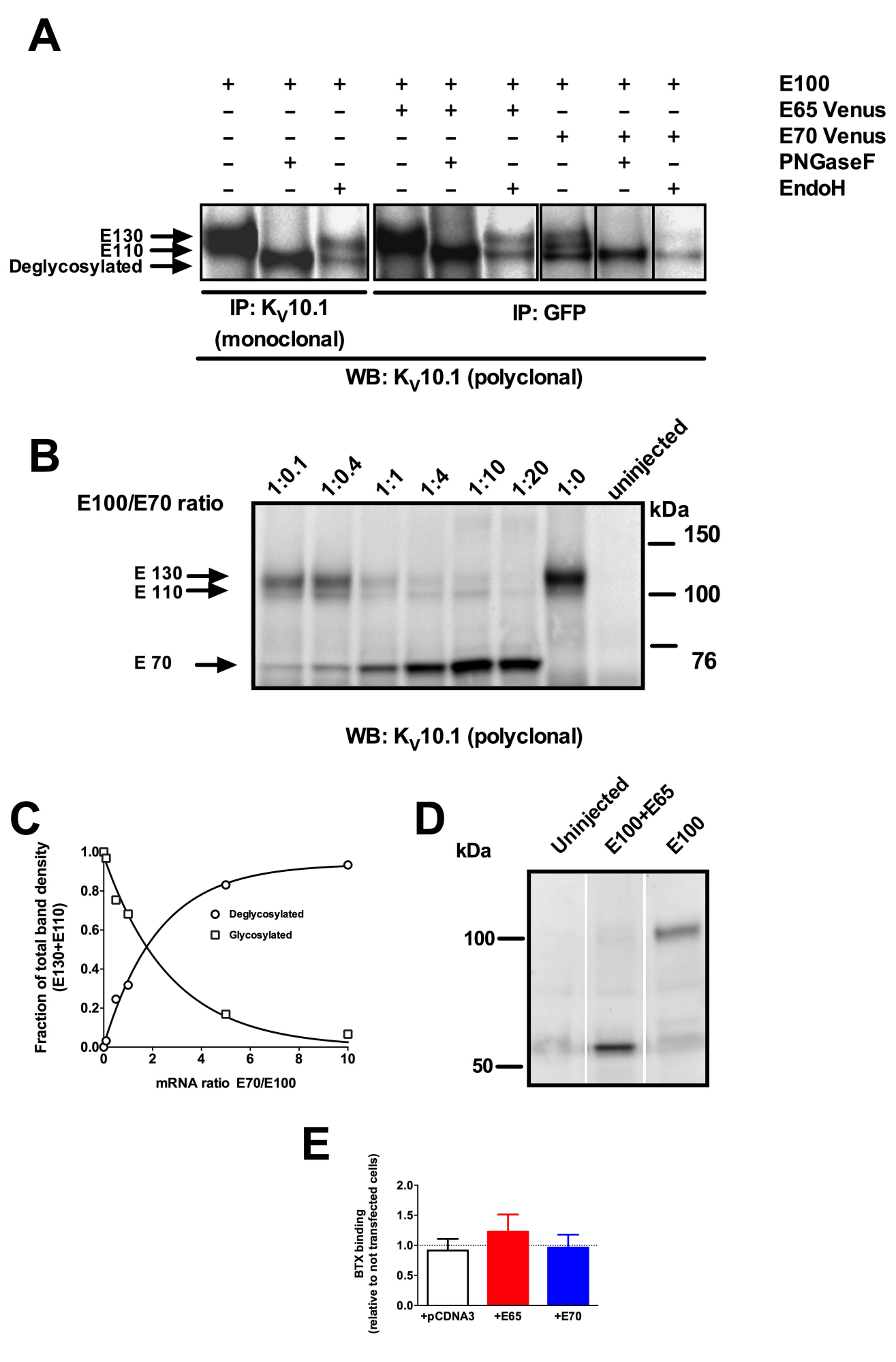
A
E100
E65 Venus
E70 Venus
PNGaseF
EndoH
E130
E110
Deglycosylated
IP: K$_V$10.1 (monoclonal)
IP: GFP
WB: K$_V$10.1 (polyclonal)
B
E100/E70 ratio
1:0.1
1:0.4
1:1
1:4
1:10
1:20
1:0
uninjected
kDa
150
100
76
E 130
E 110
E 70
WB: K$_V$10.1 (polyclonal)
C
Fraction of total band density (E130+E110)
Deglycosylated
Glycosylated
mRNA ratio E70/E100
D
kDa
Uninjected
E100+E65
E100
100
50
E
BTX binding (relative to not transfected cells)
+pCDNA3
+E65
+E70

Figure 4

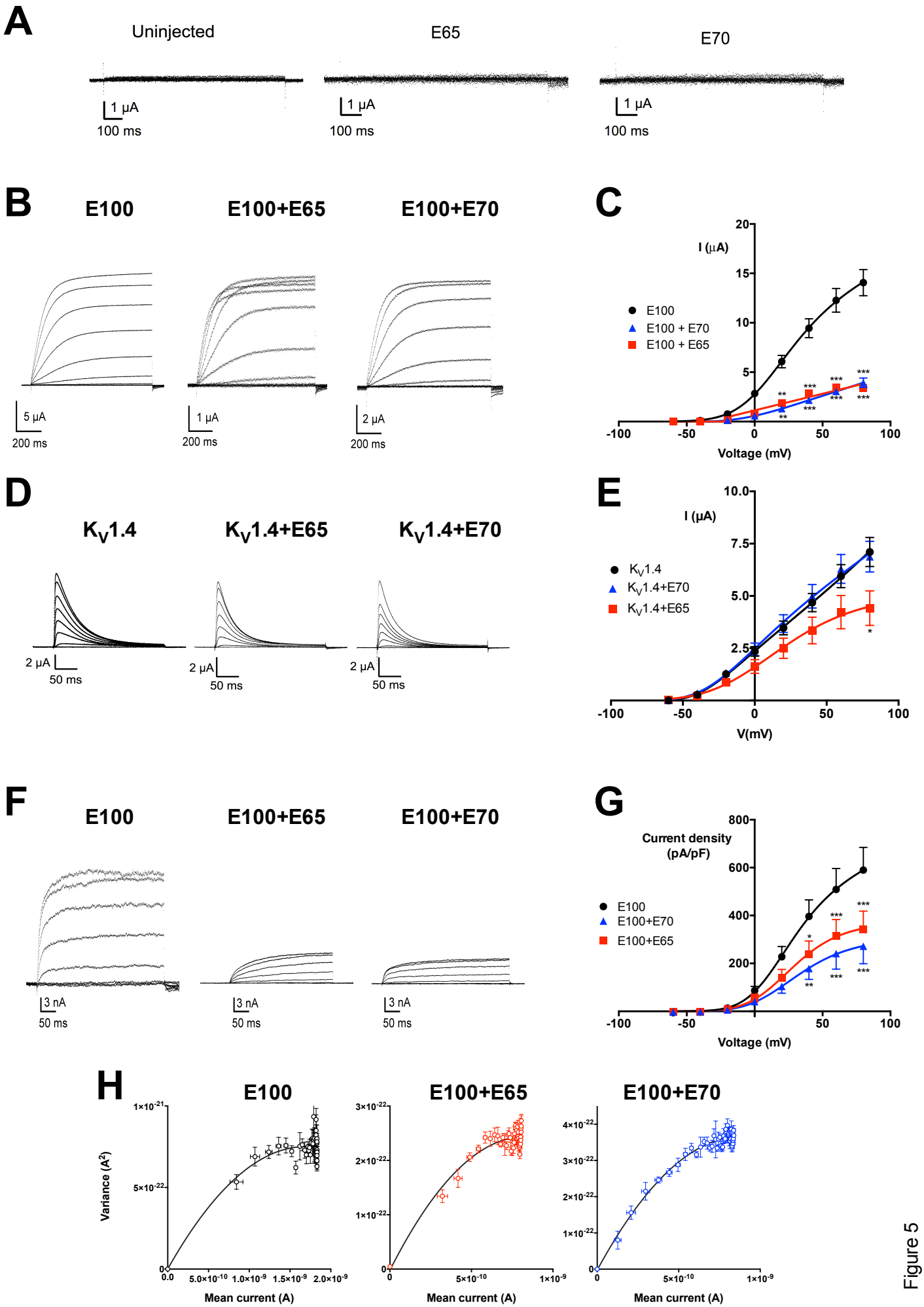
A
Uninjected
E65
E70
1 µA
100 ms
B
E100
E100+E65
E100+E70
5 µA
200 ms
1 µA
200 ms
2 µA
200 ms
C
I (µA)
E100
E100 + E70
E100 + E65
Voltage (mV)
D
K$_V$1.4
K$_V$1.4+E65
K$_V$1.4+E70
2 µA
50 ms
E
I (µA)
K$_V$1.4
K$_V$1.4+E70
K$_V$1.4+E65
V(mV)
F
E100
E100+E65
E100+E70
3 nA
50 ms
G
Current density (pA/pF)
E100
E100+E70
E100+E65
Voltage (mV)
H
E100
E100+E65
E100+E70
Variance (A^2)
Mean current (A)

Figure 5

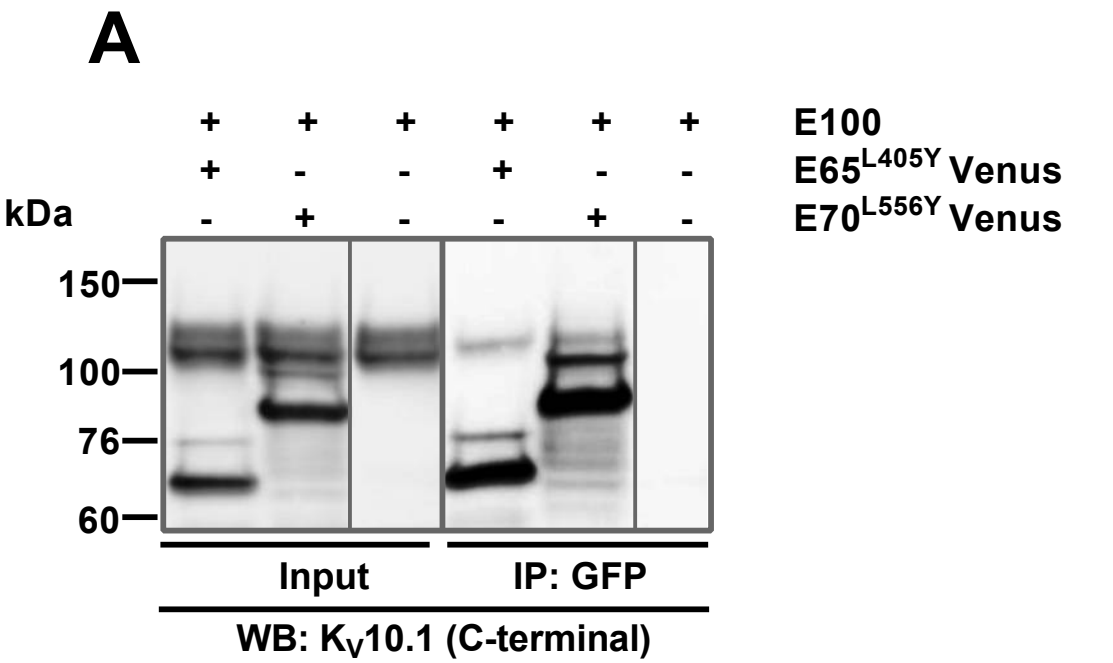
A
+ + + + + +
+ - - + - -
- + - - + -
E100
E65L405Y Venus
E70L556Y Venus
kDa
150
100
76
60
Input
IP: GFP
WB: KV10.1 (C-terminal)

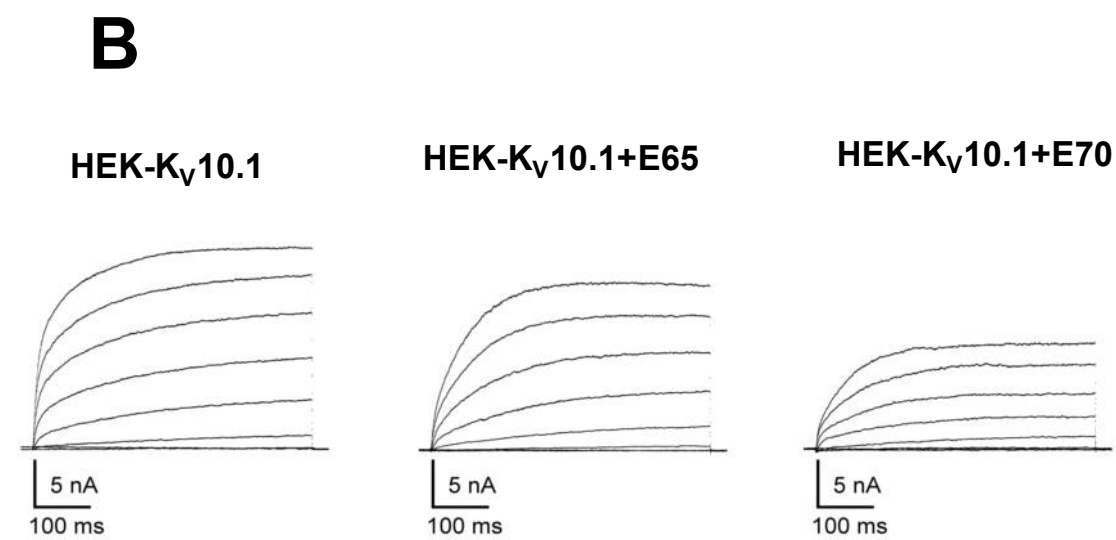
B
HEK-KV10.1
HEK-KV10.1+E65
HEK-KV10.1+E70
5 nA
100 ms
5 nA
100 ms
5 nA
100 ms

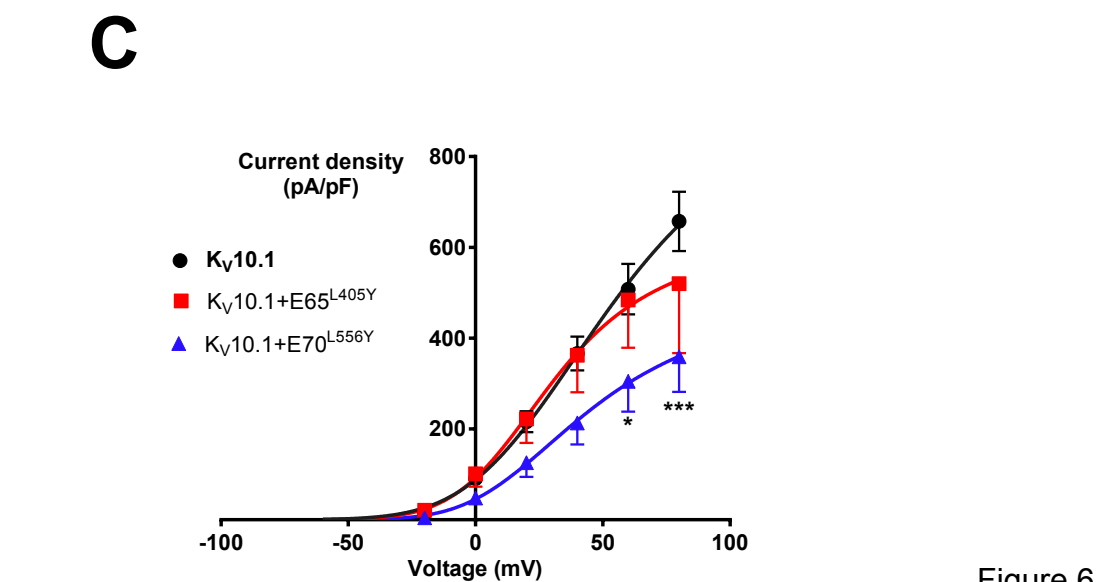
C
Current density (pA/pF)
KV10.1
KV10.1+E65L405Y
KV10.1+E70L556Y
800
600
400
200
*
***
-100
-50
0
50
100
Voltage (mV)

Figure 6

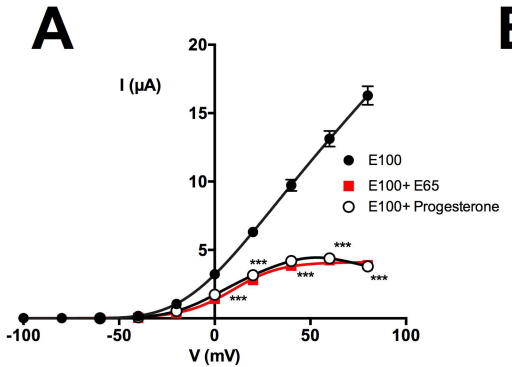
A
I (μA)
20
15
10
5
-100
-50
0
50
100
V (mV)
E100
E100+ E65
E100+ Progesterone
***
***
***
***
***

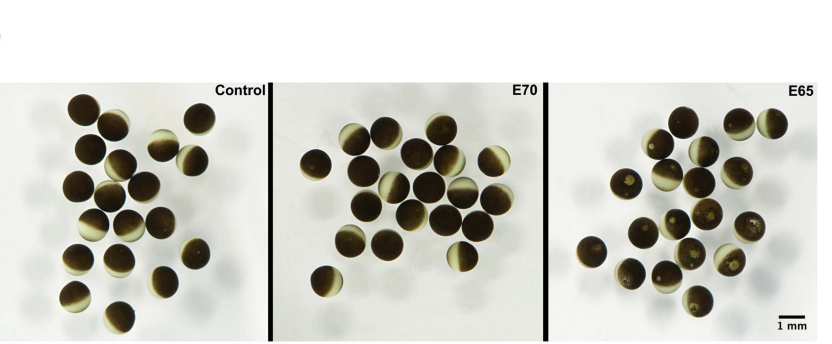
B
Control
E70
E65
1 mm

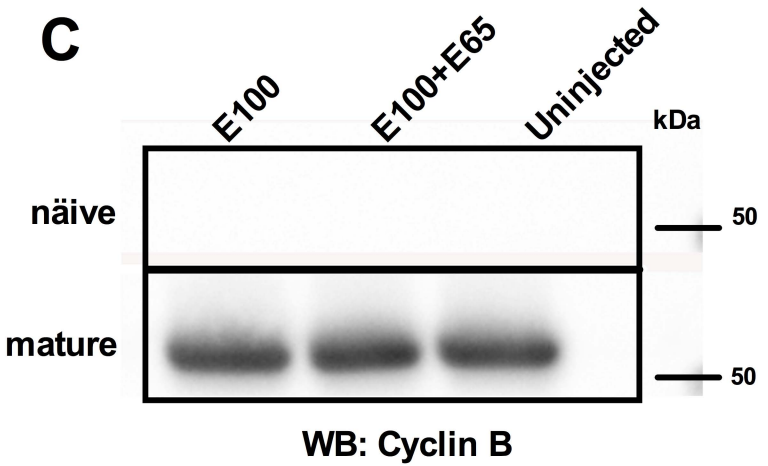
C
E100
E100+E65
Uninjected
kDa
näive
mature
50
50
WB: Cyclin B

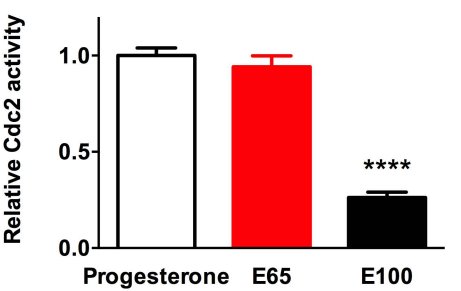
D
Relative Cdc2 activity
1.0
0.5
0.0
****
Progesterone
E65
E100

Figure 7

Cell Biology:

Alternative Spliced Isoforms of $K_V10.1$ Potassium Channels Modulate Channel Properties and can Activate Cyclin-Dependent Kinase in Xenopus Oocytes

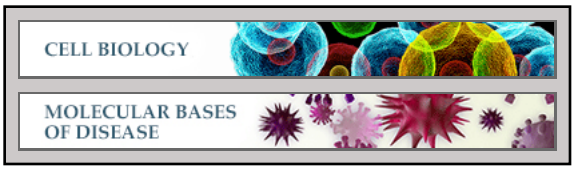

Fernanda Ramos Gomes, Vincenzo Romaniello, Araceli Sánchez, Claudia Weber, Pratibha Narayanan, Maryna Psol and Luis A. Pardo

J. Biol. Chem. *published online October 30, 2015*

Access the most updated version of this article at doi: 10.1074/jbc.M115.668749

This article cites 0 references, 0 of which can be accessed free at
http://www.jbc.org/content/early/2015/10/30/jbc.M115.668749.full.html#ref-list-1